Sustainable Chemistry and Pharmacy 19 (2021) 100353

Contents lists available at ScienceDirect

Sustainable Chemistry and Pharmacy

journal homepage: http://www.elsevier.com/locate/scp

Cleaner corrosion inhibitors using *Peumus boldus* Molina formulations in oil well acidizing fluids: gravimetric, electrochemical and DFT studies

Luana B. Furtado [a], Rafaela C. Nascimento [b], Maria José O.C. Guimarães [a], Fábio J. F. S. Henrique [c], Janaína C. Rocha [d], Peter R. Seidl [a,*], José Antônio C.P. Gomes [d]

[a] School of Chemistry, Federal University of Rio de Janeiro, Rio de Janeiro, Brazil
[b] Centro de Química de Évora, University of Evora, Évora, Portugal
[c] Chemistry Institute, Federal University of Rio de Janeiro, Rio de Janeiro, Brazil
[d] Laboratory of Corrosion, Federal University of Rio de Janeiro, Rio de Janeiro, Brazil

ARTICLE INFO

Keywords:
Corrosion inhibitors
Organic formulations
Toxic inhibitor replacement
Oil well acidizing

ABSTRACT

Eco-friendly inhibitors are an alternative to reduce environmental and human health problems related to conventional inhibitors employed in oil well acidizing. In the present study, boldo (*Peumus boldus*) was investigated as a corrosion inhibitor for API P110 carbon steel in 2 M and 15% HCl. A two-level full factorial design (2^3) was used to evaluate the extraction time (90 and 210 min), temperature (313 and 343 K) and solute/ethanol ratio (0.15 and 0.35 g of sheet/mL of ethanol). The extracts were characterized by phenolic content, Fourier-transform infrared spectroscopy, Proton nuclear magnetic resonance, relative density and refraction index. The extract concentration in 2 M HCl was evaluated at 303 and 313 K, achieving 87% efficiency. Binary formulations were developed in order to partially reduce the use of conventional inhibitors. Two formulations performed better at 333 K. Electrochemical tests provided information about the metal-solution interface in the absence and presence of the formulations, indicating that these are mixed corrosion inhibitors. Confocal microscopy elucidated metallic surface morphology. Surface characterization techniques confirmed the presence of the inhibitory film on the metallic surface. Density functional theory indicated that the boldine molecule was stable in the acidic phase, exhibiting improved anticorrosive properties.

1. Introduction

The acidizing stimulation involve the injection of an acidic solution (hydrochloric, acetic, formic, and sulfamic acids, for example) in a concentration range of 5–35%, depending on the mineral composition of the well (Rajeev et al., 2012). This procedure aims to increase well productivity, but corrosion damage is a frequent problem related to this stimulation technique (Frenier and Schlumberger, 1989).

Corrosion inhibitors can be used to protect metallic materials from corrosion damage. (Golestani et al., 2014). Inhibiting molecules must contain functional groups with electron donating atoms, *p*-type molecular orbitals, aromatic rings, and unsaturation in order to adsorb on the metallic surface (Cherrak et al., 2020; Obot and Obi-Egbedi, 2010).

Although the compounds reported in literature act as effective inhibitors, a single substance is not sufficient for an industrial application (Finsgar and Jackson, 2014). As such, multicomponent formulations containing active components that synergistically protect the materials used in oil well production must be developed (Seidl et al., 2011). Substances that may be present in these formulations include intensifiers (Ituen et al., 2016), surfactants (Mobin et al., 2016), and solvents (Finsgar and Jackson, 2014).

Since conventional inhibitors impact the environment and human health, active compounds from leaves (Dehghani et al., 2019a; Keramatinia et al., 2019; Wang et al., 2019), seeds (Bahlakeh et al., 2019; El-Etre and Ali, 2017; Dehghani et al., 2019b; Raghavendra and Bhat, 2018) and peel (Furtado et al., 2020; Singh et al., 2019; Barreto et al., 2017) have been studied as inhibitors. Green inhibitors are eco-friendly chemicals with low-level generation of hazardous substances. In addition, they are governed by sustainable chemistry with no direct or indirect negative effects on the environment (Umoren and Eduok, 2016).

Some recent works in literature have investigated corrosion inhibitors for acidic media. Ye et al. (Ye et al., 2020a) studied doped

* Corresponding author.
E-mail addresses: luana_bf18@hotmail.com (L.B. Furtado), rafaelan@uevora.pt (R.C. Nascimento), mjg@eq.ufrj.br (M.J.O.C. Guimarães), fabiojrhenrique@hotmail.com (F.J.F.S. Henrique), janaina@metalmat.ufrj.br (J.C. Rocha), peterseidl@eq.ufrj.br (P.R. Seidl), ponciano@metalmat.ufrj.br (J.A.C.P. Gomes).

https://doi.org/10.1016/j.scp.2020.100353
Received 1 August 2020; Received in revised form 24 November 2020; Accepted 2 December 2020
Available online 13 December 2020

carbon dots as corrosion inhibitors for Q235 steel in hydrochloric acid environment via weight loss test, surface characterizations and electrochemistry measurements. The authors reported electrochemical impedance efficiency of 99.35% with 200 mg/L of the inhibitor at 298 K. Functionalized carbon dots synthesized by the conjugation of imidazole and citric acid carbon dots have also been studied as corrosion inhibitors for Q235 steel in 1 M HCl solution by electrochemical analysis, corrosion morphology and adsorption isotherm. The authors indicated electrochemical impedance efficiency of 93.40% with 200 mg/L of the inhibitor (Ye et al., 2019). Ye et al. (Ye et al., 2020b) investigated novel N-doped carbon dots obtained through pyrolysis of ammonium citrate at 453 K as corrosion inhibitors for Q235 steel in 1 M HCl solution. The inhibition efficiency exceeded 90.00% at 200 mg/L. A green inhibitor of N-doped carbon dots obtained from the reaction between citric acid and L-histidine was also investigated as a corrosion inhibitor in HCl. The inhibition efficiency was above 90.00% at 100 mg/L (Ye et al., 2020c). *Eucalyptus* leaves extract was investigated as a corrosion inhibitor for mild steel in 1 M HCl, showing inhibition efficiency of 88.00% with 800 ppm after 5 h exposure (Dehghani et al., 2019a). Keramatinia, Ramezanzadeh e Mahdavian reported bio-active products from *Nettle* leaves extract as corrosion inhibitors in 1 M HCl. The authors indicated inhibition efficiency of 78.00% at 328 K after 1.50 h exposure to weight loss measurements (Keramatinia et al., 2019). Bahlakeh et al. investigated *Peganum harmala* seed extract as a corrosion inhibitor for mild steel in 1 M HCl (Bahlakeh et al., 2019). The inhibition efficiency of 94.00% in the presence of 800 ppm was achieved after 5 h immersion using EIS technique. This work focused on the extract of boldo plant, which has not been studied for this application. Besides, the advantage of the work is the development of greener formulations that partially replaces conventional inhibitors for a green source of inhibitory compounds. At last, this study reports an application more aggressive media, indicating that the formulations maintain high efficiencies.

This paper investigated the boldo plant (*Peumus boldus*) as a corrosion inhibitor for carbon steel in 2 M and 15% HCl. Although this biomass is a potential source of alkaloids and flavonoids, it has yet to be used for this application. It is important to underscore that the total alkaloid content in this biomass may vary depending on the extraction procedure, analysis method, harvest period, climatic conditions and water availability. The total alkaloid of this biomass is between 0.06% and 2.80% (Mariano, 2015), and 0.40–0.50% of this concentration belongs to the benzoquinoline class. Boldine is the main alkaloid, accounting for between 12.00 and 19.00% of total alkaloid content (Ruiz et al., 2008).

Statistical design was used to determine the best extraction conditions (time, temperature and solute/ethanol ratio) for *Peumus boldus* leaves. The extracts were characterized by phenolic content, FTIR, ^{1}H NMR, relative density and refraction index. Gravimetric measurements (2 M and 15% HCl) were performed with the optimal extract in order to investigate the possibility of partial substitution of a conventional substance by a green extract. The effect of temperature was evaluated from 303 to 373 K in 2 M and 15% HCl in order to obtain thermodynamic parameters. Electrochemical measurements elucidated the influence of the acid concentration on the inhibitory efficiency. The metallic surface was characterized by microscopy techniques. Density functional theory (DFT) studies were performed in order to determine the quantum parameters of boldine in its neutral and protonated phase, and correlate them with the experimental results obtained.

2. Experimental methodology

2.1. Extraction optimization and characterization

Dried leaves were comminuted and employed in the extraction process in order to maximize phenolic content. A two-level full factorial design (2^3) was used, with 2 replicates at the central point, totaling 10 extractions. The factors employed were time (90 and 210 min), temperature (313 and 343 K) and leaf mass ratio by volume of ethanol (0.15 and 0.35 g/mL). The refractive index (RI) of the extracts was the response variable. Data analysis was performed in Statistica software (version 13.4.0.14), with a 90% confidence interval ($\alpha = 0.10$). The RI was determined in an Abbe Q 767B bench refractometer (Quimis), with a thermometer (273–343 K) and RI measuring range between 1.300 and 1.700.

The extracts were concentrated by evaporation. Folin-Ciocalteu method was performed to determine the phenolic content (Falcão et al., 2007). A calibration curve (5 points - 100 to 500 mg/L) with gallic acid (GAE) was obtained. The equation of the calibration curve was: $y = 0.00177\ x - 0.12330$ ($R^2 = 0{,}96110$) (x = [GAE] (mg/L)). FTIR analysis using transmittance mode was performed on a Thermo Scientific Nicolet iS5 spectrometer with Fourier transform (293 K, 20 scans, 4000- 650 cm^{-1} and 4 cm^{-1} resolution). The optimized extract was analyzed by ^{1}H NMR in deuterated chloroform using a Varian Mercury VX 300 instrument, operating with a Universal 5 mm probe at 313 K and 299.99 MHz.

The relative density of the extracts was determined with a 25 mL pycnometer (Pires et al., 2015). A Shimadzu AUY 220 scale was used to measure mass (±0.10 mg).

2.2. Weight loss measurements

Carbon steel API P110 with the following composition (% w) was used in the tests: C, 0.280; Mn, 1.220; Si, 0.280; P, 0.016; S, 0.002; Ni, 0.010; Mo, 0.110; and Fe, 98.1. Test coupons measuring 8 mm × 20 mm x 5 mm with a center hole (3 mm) were prepared according to ASTM G31 (American Society for Testing and Materials, 1972). The test samples were abraded, washed in distilled water, degreased in acetone, dried and kept in desiccators prior to each test. After weighting accurately with sensitivity of ±0.10 mg, the specimens were tested in a 300 mL autoclave. Acidification tests were carried out with different concentrations of *Peumus boldus* optimal extract (B) and formulations containing this extract and conventional inhibitors (B + PA (Propargyl alcohol), B + H (5-hexyn-1-ol), B + P (2-pentyn-1-ol) and B + KI (potassium iodide)). The tests were performed at temperatures of 313 to 373 K for 24 h. The acid solution used contains 2 M or 15% hydrochloric acid and 15% butyl glycol. After the exposure, the specimens were taken out, rinsed thoroughly with distilled water, dried and weighted again. In this study, averages of two replicate values are reported. Mass loss was used to calculate the uniform corrosion rate according to ASTM G31 (American Society for Testing and Materials, 1972), as shown in Equation (1), where K is a constant, Δm is the weight loss of the sample, A is the superficial area, ρ is the density of the sample, and t is the immersion time.

$$CR = \frac{K^{*}\Delta m(g)}{A\ (cm^2)^{*}\rho\ \left(\frac{g}{cm^3}\right)^{*}t\ (h)} \quad (1)$$

The inhibiting efficiency (IE_{WL}) is calculated according to Equation (2), where CR_0 and CR_{inh} are the corrosion rates in the absence and presence of inhibitor, respectively.

$$IE_{WL}(\%) = \left(\frac{CR_0 - CR_{inh}}{CR_0}\right)^{*}100 \quad (2)$$

2.3. Electrochemical measurements

Electrochemical measurements were performed at 333 ± 1 K using a silver/silver chloride (Ag/AgCl) electrode as the reference electrode and a platinum wire as the counter electrode. A salt bridge was used to separate the reference medium from the aggressive medium. B, B + PA, B + H, B + P and B + KI formulations were evaluated at 333 K in 2 M and 15% HCl. The open circuit potential was recorded for 30 min. Electrochemical impedance spectroscopy (EIS) was performed with a peak amplitude of 10 mV in the 10 kHz to 10 mHz frequency range. The

polarization scanning rate was 0.33 mV s^{-1} in the anodic and cathodic directions (E = Ecorr ± 250 mV). Polarizations were measured in duplicate, and OCP and impedance in quadruplicate. The experiments were performed with a computer-controlled instrument (Autolab Potentiostat/Galvanostat (PGSTAT302)) in NOVA software 1.11.

2.4. Scanning electron microscopy (SEM-EDX), confocal laser scanning microscopy and FTIR-ATR

The carbon steel samples after immersion tests with and without the formulations (B + PA and B + H) at 333K for 24 h were analyzed by SEM-EDX using a Hitachi TM 3030 Plus tabletop scanning electron microscope. These samples were also analyzed on a ZEISS LSM 800 MAT confocal laser scanning microscope with Zen 2.3 Blue edition software. The inhibitory films (B + PA and B + H) on the metallic surface were analyzed using a Perkim Elmer Spectrum 100 series Fourier transform infrared spectrometer (FTIR-ATR). A total of 32 scans were collected in the 4000 to 650 cm^{-1} range, at a spectral resolution of 4 cm^{-1}.

2.5. Molecular modeling

Complete geometric optimization of the alkaloid boldine (Fig. 1) in neutral and protonated form was performed using density functional theory (DFT) in the gas phase. The B3LYP functional and 6-31G(*d,p*) base function were used to describe all atoms, implemented by the Gaussian 09 program package (Frisch et al., 2009). The energies of the highest (E_{HOMO}) and lowest (E_{LUMO}) occupied molecular orbitals, energy gap (ΔE), hardness (η) and softness (σ) were calculated. Mulliken charges (HOMO and LUMO orbitals) were obtained for neutral and protonated molecules.

3. Results

3.1. Statistical design

The factors and the response variable (refraction index) analyzed in the statistical design are shown in Table 1. The Pareto chart (Fig. 2 (a)) shows that all factors are significant and that the solute/ethanol ratio exhibited the greatest influence. Fig. 2 (b), 2 (c) and 2 (d) illustrate the response surfaces as a function of the evaluated factors, which are coded so that 1 corresponds to the maximum and −1 to the minimum level of each factor. Fig. 2 (b) demonstrates that when the mass ratio is set at 1, the response increases linearly at the highest temperature, showing little influence of time. Fig. 2 (c) shows that by setting the temperature to 1, the maximum response is for the largest mass ratio, with little influence of time. Thus, according to the Pareto chart (Fig. 2 (a)), despite being significant, time extraction has a small influence on the refraction index, as demonstrated in Fig. 2 (b) and (c). Fig. 2 (d) shows that when setting the time to 1, the maximum response occurs when the temperature and solute/ethanol ratio are at the upper limit of the evaluated range. Thus, the optimal extraction condition in the evaluated range occurs at the maximum values studied for temperature and solute/ethanol ratio, that is, at 210 min of extraction, 343 K and 0.35 g of solute per mL of solvent. The pure error obtained by the ANOVA test was 1.25E-07, and the lack of fit was 3.71E-07. The ANOVA test is presented in Table 2, confirming that the model is significant as confirmed by the p value.

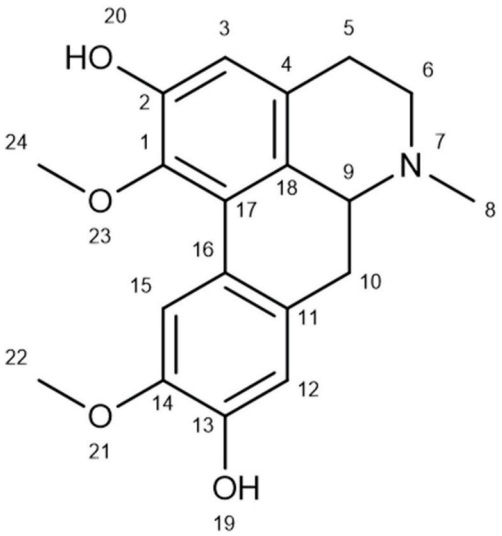

Fig. 1. Boldine structure. ($C_{19}H_{21}NO_4$).

Table 1
Factors and response variable used in the 2^3 statistical design for the optimization of *Peumus boldus* extraction.

Tests	Time (min)	Temperature (K)	Solute/ethanol ratio (g/ml)	Refraction index
1	90	313	0.15	1.3649
2	210	313	0.15	1.3672
3	90	343	0.15	1.3676
4	210	343	0.15	1.3689
5	90	313	0.35	1.3701
6	210	313	0.35	1.3704
7	90	343	0.35	1.3736
8	210	343	0.35	1.3736
9	150	328	0.20	1.3687
10	150	328	0.20	1.3692

3.2. Extract characterization

3.2.1. Phenolic content and relative density

Table 3 shows the phenolic content for each extract obtained with the gallic acid calibration (Fig. 3). A calibration curve was constructed with the standard gallic acid using five concentrations of this reagent (100 to 500 mg/L). Absorbance was measured at each concentration, which allowed the construction of the graph in Fig. 3. The calibration curve was obtained from this graph that correlates gallic acid concentration and absorbance. Then, absorbance was measured for each extract shown in Table 3. The phenolic concentration of each extract was calculated from the absorbance values and the calibration curve obtained before.

The center points (150 min, 328 K and 0.20 g of solute/mL of ethanol) showed similar concentration values (coefficient of variation of 1.09%), revealing good extraction reproducibility. The concentrations of phenolics increased with a rise in the variables under study, reaching a maximum value at the optimal statistical design condition (210 min, 343 K and 0.35 g of leaves/mL of ethanol).

When extracts are compared using the same time and temperatures, varying only the solute/ethanol ratio, such as 90 min, 343 K, 0.15 g/mL-90 min, 343 K, 0.35 g/mL, there is a significant increase in relative density, which is correlated to greater compound extraction. It can be concluded that higher relative density corresponds to higher phenolic content, since relative density is a consequence of the phenolic concentration.

3.2.2. FTIR

Only 4 spectra from Table 3 (related to the highest phenolic content) were selected for the FTIR analysis. The FTIR technique revealed the following bands in the concentrated extracts (Fig. 4(a)-(d)): OH stretching (3043 cm^{-1}), symmetrical/asymmetrical CH stretching (2959 cm^{-1}), symmetrical/asymmetrical methylene stretching (CH_2) (2919 and 2850 cm^{-1}), angular deformation of the aromatic ring (1516, 1463 and 1456 cm^{-1}) (Edelmann and Lendl, 2002; Oliveira et al., 1999), phenol or tertiary alcohol (1377 cm^{-1}), C═C (1682 cm^{-1}), C–H

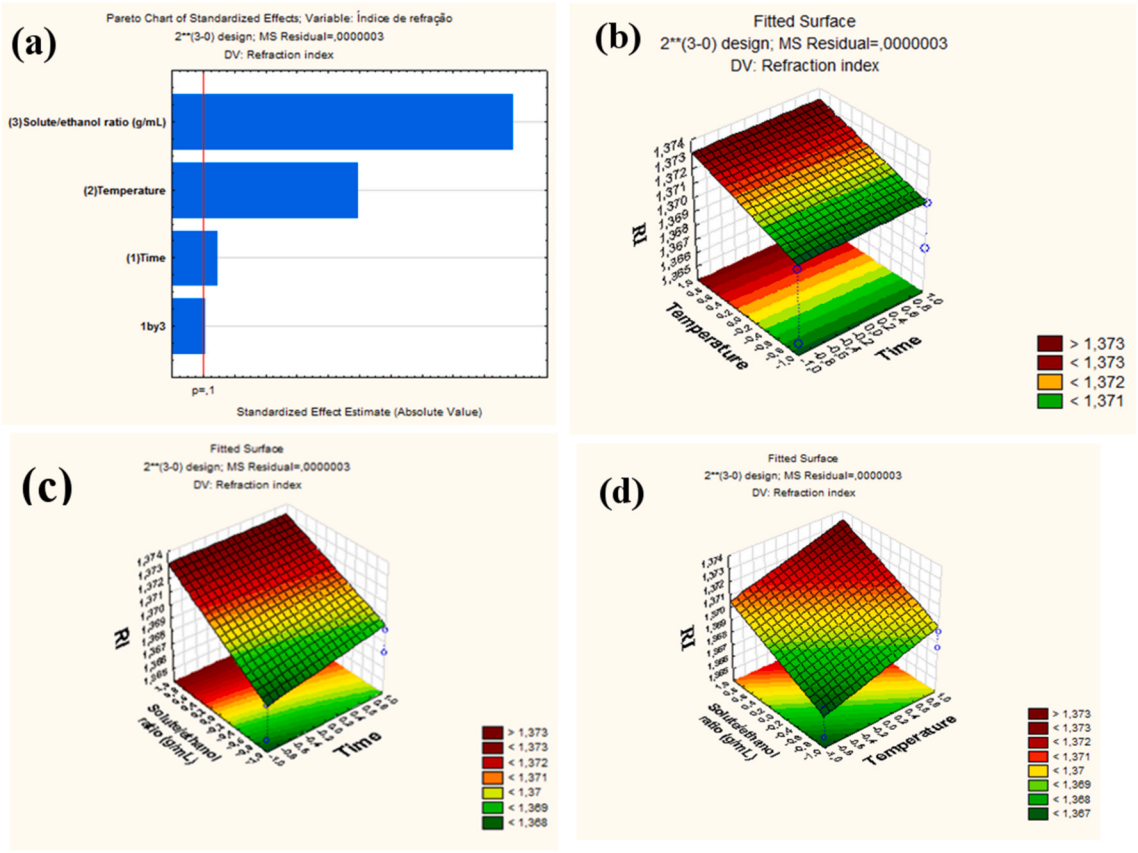

Fig. 2. (a) Pareto chart; (b) Response surface as a function of temperature and time, fixing leaf mass/volume of ethanol ratio; (c) Response surface as a function of leaf mass/ethanol volume ratio and time, setting temperature; and, (d) Response surface in terms of leaf mass/ethanol volume ratio and temperature, setting time.

Table 2
ANOVA test for the statistical design.

ANOVA	Sum of squares (SQ)	Degrees of Freedom	Mean Square	F	P
REGRESSION	6.43E-05	4	1.60E-05	49.86	3.22E-04
RESIDUE	1.61E-06	5	3.22E-07		
LACK OF FIT	1.49E-06	4	3.71E-07		
PURE ERROR	1.30E-07	1	1.25E-07		
SQ TOTAL	6.59E-05	9	7.31E-06		

Table 3
Phenolic concentration values (mg GAE/mL) obtained using the Folin-Ciocalteu technique.

Time (min)	Temperature (K)	Leaf mass (g)/ ethanol volume (mL)	Phenolic concentration (mg GAE/L)	Relative density (g/ cm^3)
90	313	0.15	2941	0.8247
210	313	0.15	3007	0.8222
90	343	0.15	3152	0.8239
210	343	0.15	3179	0.8253
150	328	0.20	3535	0.8281
150	328	0.20	3613	0.8290
210	313	0.35	3718	0.8351
90	343	0.35	3829	0.8454
90	313	0.35	3885	0.8363
210	343	0.35	3935	0.8455

aromatic angular deformation on the plane (1080 and 1049 cm^{-1}) (Fernández and Agosin, 2007), and aromatic CH angular deformation off the plane (880, 848, 729, 720 and 698 cm^{-1}) (Coates, 2006). This

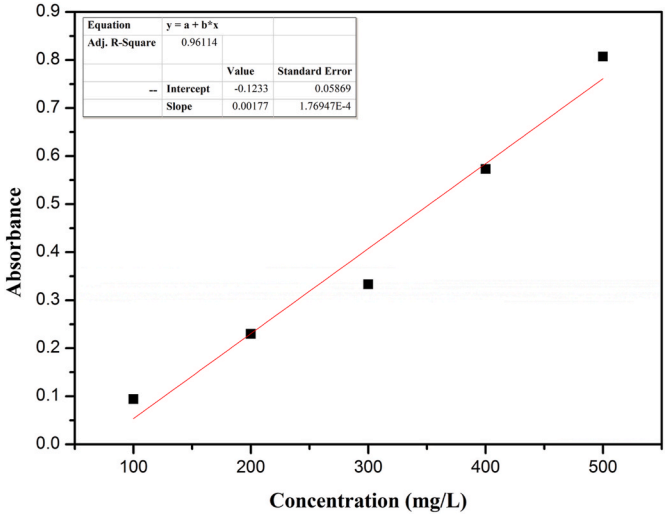

Fig. 3. Calibration with gallic acid between 100 and 500 mg/L.

demonstrates that the constituents of boldo are phenolic compounds and unsaturated carbon chains. In addition, all the extracts exhibit bands in very similar regions, indicating that extraction conditions have influenced in the concentration of the extracted compounds, but not in the type of compound extracted.

3.2.3. ^1H NMR

The ^1H NMR technique (Fig. 5) used for the optimized extract (210 min, 343 K and 0.35 g of solute/ml of ethanol) revealed peaks at

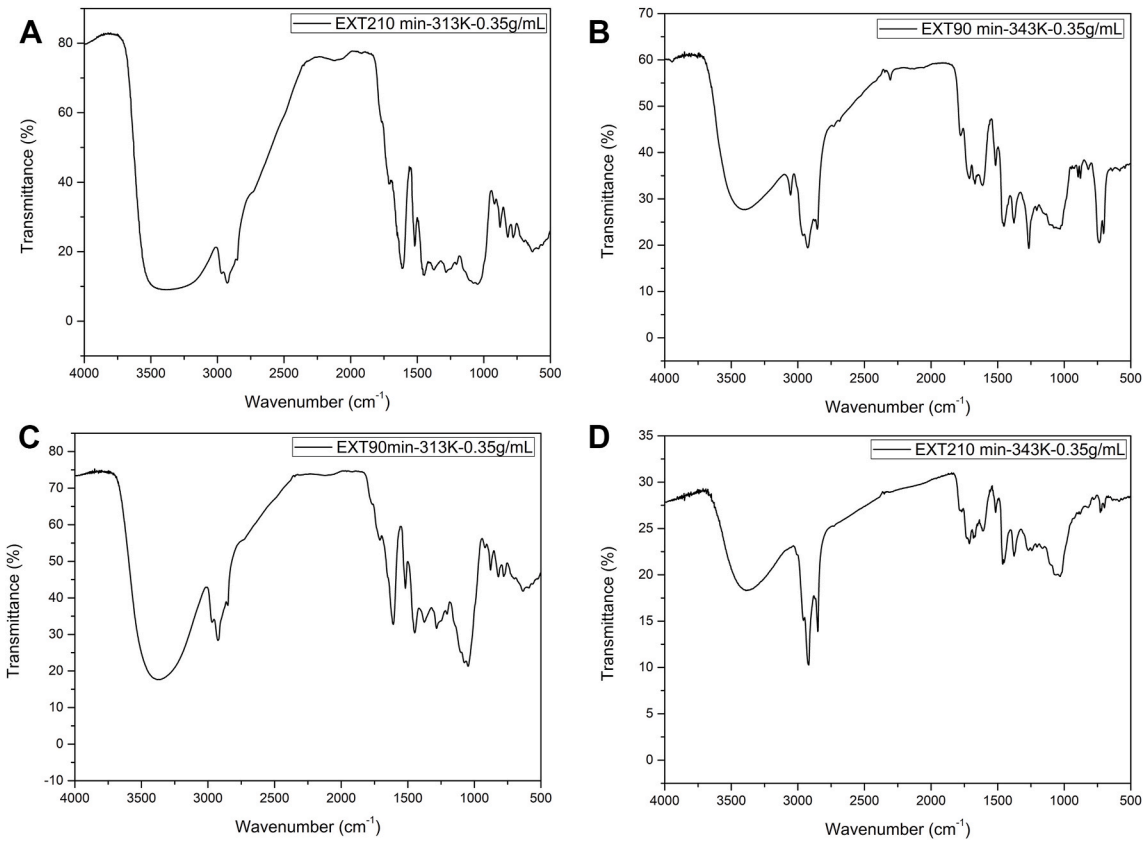

Fig. 4. FTIR spectra for the extracts under the following conditions: (a) 210 min, 313 K, 0.35 g/mL; (b) 90 min, 343 K, 0.35 g/mL; (c) 90 min, 313 K, 0.35 g/mL; (d) 210 min, 343 K, 0.35 g/mL.

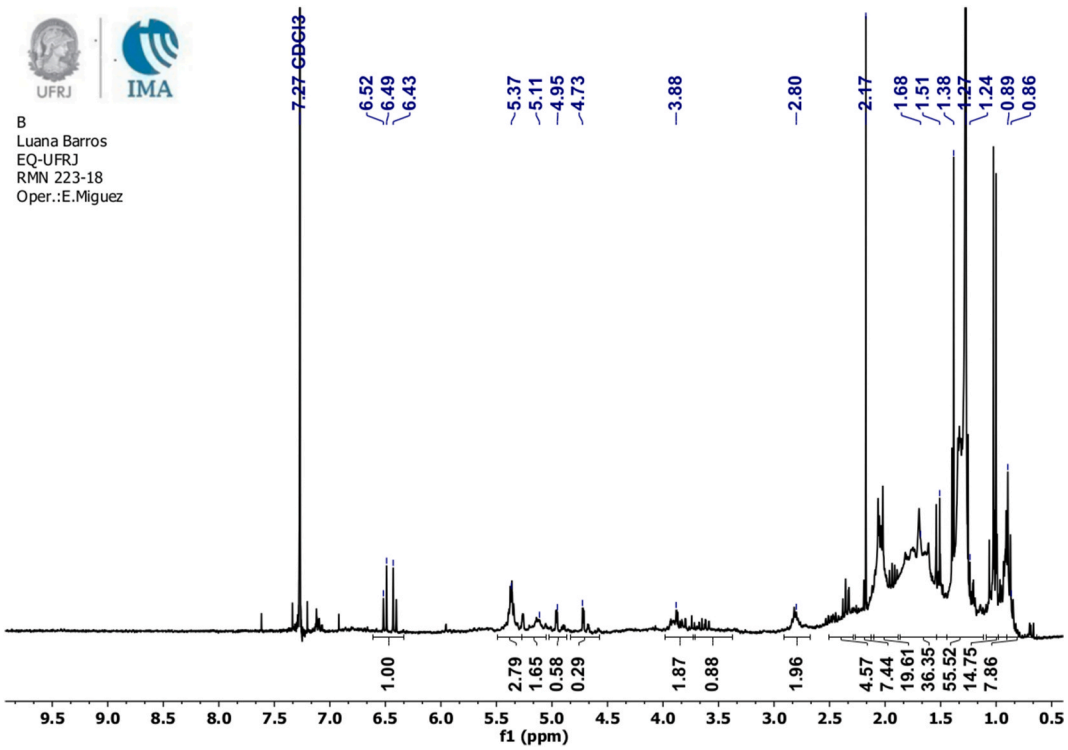

Fig. 5. ^{1}H NMR of the extract obtained in the optimal condition.

0.86–0.89 ppm referring to terminal methyl (R–CH_3); peaks at 1.24–1.38 ppm in relation to aliphatic hydrogens (R–CH_2 –R); peaks at 1.51–1.68 for methyl groups; peak at 2.17 ppm for R–$COCH_3$; at 2.80 ppm for bis-allylic methylene groups; 3.88 ppm in relation to RO-CH_3; between 5.11 and 5.37 ppm for non-terminal olefin hydrogens (R_2C = CHR); and between 6.43 and 6.52 ppm for aromatic hydrogens (Pavia et al., 1996). There is also a significant presence of aliphatic hydrogens. This analysis corroborates the data obtained by FTIR, confirming the presence of aliphatic and aromatic compounds.

3.3. Weight loss measurements

The optimized extract was concentrated on a heating plate for 1 h at 353 K, obtaining a viscous liquid. This liquid was mixed with ethanol using the same mass ratio. This formulation (B) was studied at 303 and 313 K in a range of 0–4.00% w/v. The correlation between weight loss and CR/E_{WL} can be found in section 2.2, equations (1) and (2). Table 4 shows that high efficiencies (E_{WL}) were maintained as the temperature increased. The maximum efficiency (87.15%) at 313 K was at a concentration of 1.20% w/v. The concentration was extrapolated to 4.00% w/v in order to determine if the ideal concentration range of this inhibitor was higher. However, the ideal concentration identified was 1.20% w/v. This test showed that *Peumus boldus* extract is a corrosion inhibitor with efficiencies comparable to those reported in other studies (Santos et al., 2019; Souza et al., 2016).

The next step consisted of evaluating the effect of combining *Peumus boldus* extract at a concentration of 1.20% w/v with conventional inhibitors in binary formulations. The purpose of this mixture is to investigate the possibility of total or partial replacement of conventional inhibitors for a green counterpart.

The conventional inhibitors selected were propargyl alcohol (PA), 5-hexyn-1-ol (H), 2-pentyn-1-ol (P) and octin-3-ol (O). The effect of potassium iodide (KI) was also investigated. It should be emphasized that these alcohols are related to environmental problems and have been used in patented inhibitory formulations for oil well acidizing for more than five decades (Finsgar and Jackson, 2014; Mesher, 2006; Funkhouser et al., 2001; Williams et al., 1996; Aribo et al., 2017). Moreover, studies have reported concentrations up to 2.00%wt (Menezes et al., 2007; Hill, 2014; Oliveira, 2002). of these conventional inhibitors. Thus, these compounds were used in conjunction with formulation B at a fixed concentration (0.15% w/v) to evaluate the decline in corrosion rates promoted by the additive effect of the compounds. This effect is shown as a decrease in CR in Table 5. In the present study, these compounds were used at concentrations 13 times lower than usual.

Table 5 shows the corrosion rate decrease (%) of the binary formulations containing B in relation to the respective conventional inhibitor. The binary formulations reduced the corrosion rate by more than 23.00% due to an additive effect of the compounds, except for octin-3-ol (O). Since octin-3-ol has the largest carbon chain between the conventional substances, it can be concluded that there was a competition between the extract compounds and O. As such, there was no gain in efficiency and no additive effect was observed. The most significant decline in corrosion rate was with 5-hexyn-1-ol (42.85%). This can be explained by the carbon chain of the conventional inhibitor structure. 5-hexyn-1-ol has a longer carbon chain than PA and P, and shorter than O. The CR decline increased with the carbon chain of the conventional inhibitor, reaching a maximum with H. A further increase in carbons (O) has no effect, due to greater competition. Thus, the optimal carbon chain of the conventional structure is with H, allowing greater coating when associated with *Peumus boldus* extract. As such, it allows easier anchoring to the metal surface. The B + KI formulation accounted for the greatest reduction in corrosion rate when compared to the conventional inhibitor alone (44.68%). Despite this reduction, the B + KI formulation was much less efficient than the formulations containing acetylenic alcohols (89.59%).

Table 4
Corrosion rates (mm/year) and efficiencies (%) of formulation B in 2 M HCl at 303 and 313 K.

Concentration of formulation B (%w/v)	303 K		313 K	
	CR (mm/y)	E_{WL} (%)	CR (mm/y)	E_{WL} (%)
0.00 (Blank)	7.58	–	14.97	–
0.60	1.22	83.88	2.38	84.09
0.80	1.02	86.59	2.47	83.48
1.00	1.17	84.58	2.51	83.24
1.20	1.01	86.61	1.92	87.15
4.00	0.91	87.60	2.09	86.01

Table 5
Corrosion rates (mm/y) and efficiencies (%) of formulations containing conventional inhibitors in 2 M HCl at 313 K.

Formulations	CR (mm/y)	E_{WL} (%)	Decrease in CR (%) in relation to the conventional inhibitor
B (1.20 %w/v)	1.92	87.15	–
B (1.20 %w/v) + PA (0.15 %w/v)	0.33	97.79	23.25
B (1.20 %w/v) + P (0.15 %w/v)	1.05	92.54	29.05
B (1.20 %w/v) + H (0.15 %w/v)	0.32	97.86	42.85
B (1.20 %w/v) + O (0.15 %w/v)	0.19	98.69	0.00
B (1.20 %w/v) + KI (0.15 %w/v)	1.56	89.59	44.68

The effects of temperature (323–373 K) and acid concentration (2 M and 15% HCl) were evaluated for the binary formulations (B + PA, B + H, B + P, B + KI) presented in Table 5. Total mass loss (TML) was observed for the blank under some conditions (353 K in 15% HCl, and 373 K in 2 M and 15% HCl). For this reason, efficiencies at these temperatures were not calculated, as seen in Table 6. Analysis of each formulation reveals an increase in corrosion rates with temperature. For instance, with B + PA, the corrosion rate increased 9 times in 2 M HCl and 17 times in 15% HCl over the 323–373 K temperature range. In addition, in 2 M HCl, formulation B showed 83.00–88.00% efficiencies at 323–333K. Despite being lower in 15% HCl, formulation B efficiencies are in good agreement with other literature studies (Umoren et al., 1080; Biswas et al., 2015). Thus, it is clear that natural inhibitors exhibit reduced efficiency in 15% HCl, reaffirming the need to develop multicomponent formulations.

The formulation with KI is not as efficient as formulation with acetylenic alcohols, despite being reported for acidizing operations (Menezes et al., 2007). Among the formulations with acetylenic alcohols, B + PA exhibits the lowest corrosion rates from 323 to 373 K. The B + H formulation shows corrosion rates similar to those of B + PA in 15% HCl up to 333 K. It is important to underscore that acidizing operations require corrosion rates below 5 mm/y (Joia et al., 2001). Based on this criterion, formulations B + PA and B + H could be employed up to 333 K in 15% HCl. It should be mentioned that in 2 M HCl (equivalent to 5% HCl acidizing operation), B + PA corrosion rates remain below 5 mm/y up to 373 K.

Although a totally green formulation such as B was not able to act alone in 15% HCl within the corrosion rate criterion, the extract significantly reduced the use of conventional substances. Ajayi, Everitt and Voisey (Ajayi et al., 2017) reported 99.00% efficiency of PA in 15% HCl (333 K) after 24 h exposure of mild steel. The PA concentration was 7 g/L. In this respect, the B + PA formulation achieved the same efficiency reported by these authors, applying a PA concentration 4.7 times lower. In relation to a number of other authors that reported concentrations of 2.00%w/v (Menezes et al., 2007; Hill, 2014; Oliveira, 2002), there was a 13-fold decrease. . The concentration was designed to be the lowest possible to maintain good reproducibility in corrosion tests.

Table 6
Corrosion rates (mm/y) and efficiencies (%) of B + PA, B + H, B + P, B + KI and B formulations from 323 to 373 K in 2 M and 15% HCl.

	323 K				333 K				353 K				373 K			
	2 M		15%		2 M		15%		2 M		15%		2 M		15%	
	CR (mm/y)	IE (%)	CR (mm/y)	IE (%)	CR (mm/y)	IE (%)	CR (mm/y)	IE (%)	CR (mm/y)	IE (%)	CR (mm/y)	IE (%)	CR (mm/y)	IE (%)	CR (mm/y)	IE (%)
Blank	30.78	–	69.35	–	80.11	–	145.59	–	222.08	–	TML	–	TML	–	TML	–
B + PA	0.49	98.42	0.90	98.69	0.56	99.29	1.36	99.07	3.31	98.51	8.98	–	4.47	–	15.46	–
B + H	0.51	98.35	1.20	98.27	0.85	98.94	2.06	98.58	3.92	98.24	305.77	–	9.25	–	327.52	–
B + P	2.01	93.48	5.16	92.56	4.13	94.84	7.43	90.72	9.40	95.76	30.16	–	26.05	–	204.44	–
B + KI	3.66	88.12	14.46	79.14	8.77	89.05	51.16	64.86	43.60	80.36	250.73	–	82.90	–	TML	0
B	5.22	83.04	36.39	47.53	9.25	88.44	87.55	39.86	72.56	67.33	196.51	–	149.41	–	TML	0

TML -total mass loss.

At 353 K, the corrosion rate increased significantly for B + H and B + KI, which exhibited a higher CR than B. The additive effect of these formulations was observed only up to 333 K at 15% HCl.

3.3.1. Thermodynamic parameters

The effect of temperature was evaluated using the Arrhenius equation (Eq. (3)) in order to obtain the activation energies for formulations whose corrosion rates were studied from 313 to 333 K (Table 7).

$$\log CR = \frac{-E_a}{2.303\,RT} + \log A \quad (3)$$

where CR is the corrosion rate, E_a the apparent activation energy of the dissolution of carbon steel, R the molar constant of the gases, T the absolute temperature, and A the pre-exponential factor. Fig. 6(a) and (b) show the straight lines with a slope of (E_a/2.303R) from which E_a values were computed. The regression coefficients for all assays in 15% HCl (Fig. 6(b)) were in the range of 0.97–0.99, indicating that the corrosion of carbon steel in HCl can be explained with a reasonable degree of certainty using the kinetic model.

It is observed a reduction in apparent activation energy for all formulations, except for formulations B + KI and B (Table 7). This change in E_a in the presence of additives is due to the modification of the corrosion mechanism in the presence of adsorbed inhibitor molecules. In general, higher E_a values in the presence of additives are related to physical adsorption mechanism, which leads to electrostatic adsorption films. Lower E_a values for inhibited systems compared to the blank are related to the chemisorption mechanism (Santos et al., 2019; Gowraraju et al., 2017). Thus, it can be stated that formulations B + PA, B + H and B + P adsorb chemically, while B + KI and B adsorb physically. The higher corrosion rates exhibited by formulations B + KI and B and, consequently, lower inhibition efficiencies can be explained by physical adsorption. This type of adsorption, especially at high temperatures, tends to be less effective for metallic protection.

3.4. Electrochemical measurements

Nyquist diagrams were obtained for API P110 carbon steel in 2 M and 15% HCl in the presence and absence of the inhibiting formulations, according to Fig. 7. The parameters obtained by electrochemical impedance spectroscopy (R_s-resistance of the solution; R_{ct}-charge transfer resistance; C_{dl}-electric double layer capacitance; E_{EIS}- inhibition efficiency) are shown in Table 8. It should be mentioned that no equivalent circuit was used in this work and the parameters were obtained directly from the capacitive arcs. The approach and adsorption of an organic compound at the metal-solution interface displace the water molecules initially adsorbed on the metal, modifying the double electric layer composition and structure (Mishra et al., 2018).

Fig. 7 (a) and (b) show larger arcs for B + PA, followed by B + H, reflecting the order of efficiency observed in the gravimetric tests. These formulations containing acetylenic alcohols exhibited inductive arcs at low frequencies in 15% HCl. An inductive arc is generally attributed to adsorbed Fe(I) and Fe(II) intermediate species in HCl solutions. These arcs may also be attributed to the relaxation process obtained by adsorbing species such as Cl^-_{ads} and H^+_{ads} onto the electrode surface (Holze, 2005; Emran, 2015). In addition, these arcs are more pronounced for B + PA and B + H tests, which may correspond to intermediate species with acetylenic compounds.

The representative values of the double electric layer (C_{dl}) for all formulations, except B + P in HCl 2 M, are lower than the blank. The B + P formulation has the lowest efficiency containing acetylenic alcohol. As such, this increase in C_{dl} may be related to desorption of species (iron ions and inhibiting molecules) (Ben Aoun et al., 2016; Juttner, 1990). Moreover, C_{dl} values in 15% HCl are much higher than in 2 M for all formulations. However, the C_{dl} values of two formulations (B + PA and B + H) are especially high. These formulations showed inductive arcs at low frequencies. It can be concluded that the aggressiveness of the media results in desorption of species and double layer unpacking.

Tafel curves (Fig. 8) obtained by polarization tests indicate the current density behavior and corrosion potential in the presence of the formulations (Pereira et al., 2012). The electrochemical parameters (corrosion current density - I_{corr}; corrosion potential - E_{corr}; slope of the anode and cathode curve - β_a, β_c; and inhibition efficiency - E_{PDP}) are shown in Table 9.

According to Badea et al. (McCafferty, 2005; Badea et al., 2010; Pourbaix et al., 1973), for an accurate Tafel extrapolation, at least one of the branches of the polarization curve should exhibit Tafel behavior over at least one decade of current density and extrapolation should start at least 50 to 100 mV from E_{corr}. Since there are two anodic reactions in the B + PA and B + H curves in 2 M HCl, as indicated in Fig. 8 (a), Tafel extrapolation is not advisable. However, I_{corr} and E_{corr} displacement were analyzed.

In 15% HCl (Fig. 8 (b)), the formulations B + PA, B + H and B + P significantly displaced the I_{corr}. This displacement was more pronounced in the presence of PA, confirming EIS and gravimetric data. Since the I_{corr} decrease is more evident in 15% HCl, it can be concluded that the formulations with acetylenic alcohols perform better in a more

Table 7
Activation energies (kJ/mol) obtained for API P110 carbon steel in 2 M and 15% HCl in the absence and presence of different formulations.

Test	2 M	15%
	E_a (KJ/mol)	E_a (KJ/mol)
Blank	62.90	76.54
B + PA	52.39	37.69
B + H	58.01	47.38
B + P	51.03	38.93
B + KI	77.80	89.23
B	82.18	86.12

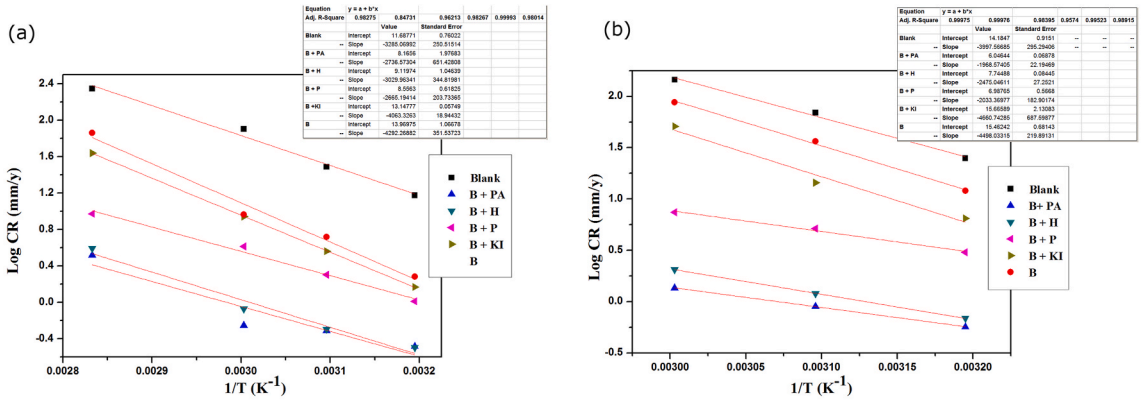

Fig. 6. Arrhenius plots for carbon steel API P110 in the absence and presence of different formulations (a) in 2 M HCl and (b) in 15% HCl.

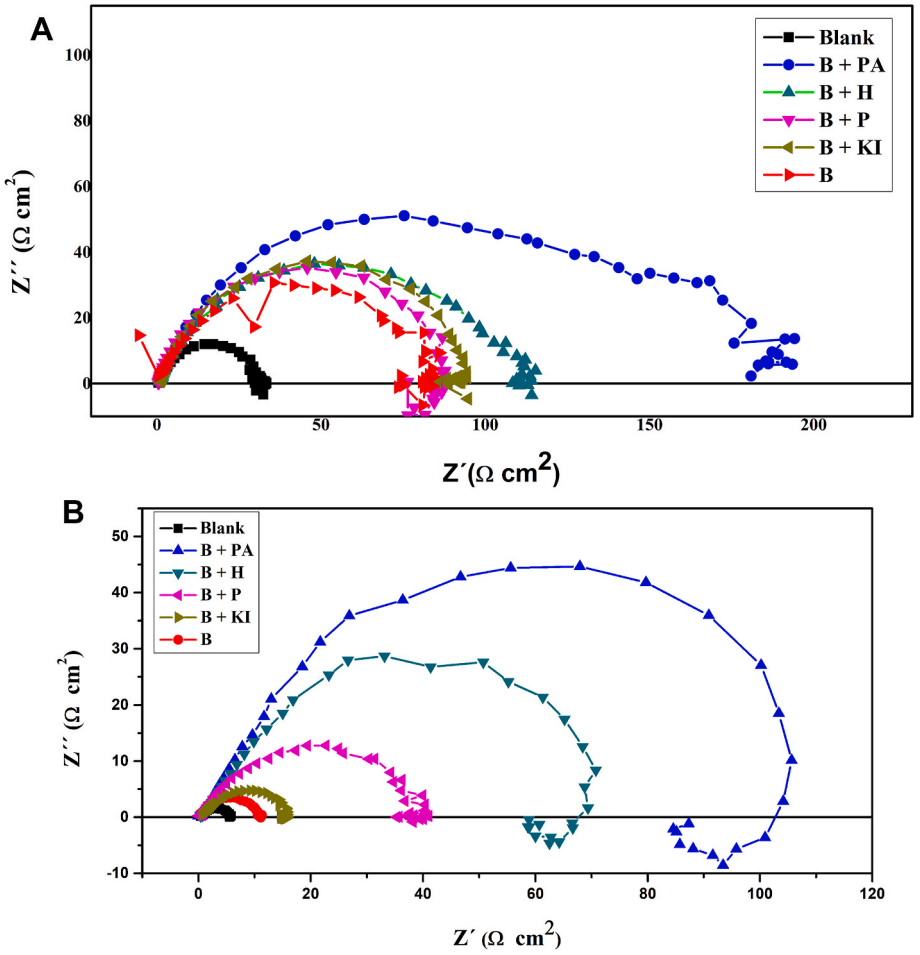

Fig. 7. EIS plots for carbon steel API P110 at 333 K in 2 M (a) and 15% HCl (b) with the blank, and formulations B + PA, B + H, B + P, B + KI and B.

Table 8
Parameters obtained by EIS for API P110 carbon steel in 2 M and 15% HCl with and without formulations B + PA, B + H, B + P, B + KI and B at 333 K.

		2 M				15%			
		R_s (Ω cm^2)	R_{ct} (Ω cm^2)	C_{dl} (μF/cm^2)	E_{EIS} (%)	R_s (Ω cm^2)	R_{ct} (Ω cm^2)	C_{dl} (μF/cm^2)	E_{EIS} (%)
Blank	0.44	33.37	101.17	–	0.35	5.54	346.72	–	
B + PA	0.79	193.46	40.67	82.91	0.01	104.16	1679.15	95.02	
B + H	0.67	108.34	72.61	69.41	0.35	69.36	1082.40	92.48	
B + P	0.35	87.67	209.15	62.28	0.01	35.75	386.79	85.48	
B + KI	0.96	92.69	84.88	64.10	0.66	14.82	227.82	63.35	
B	0.05	74.75	45.16	55.94	0.02	7.75	328.58	32.80	

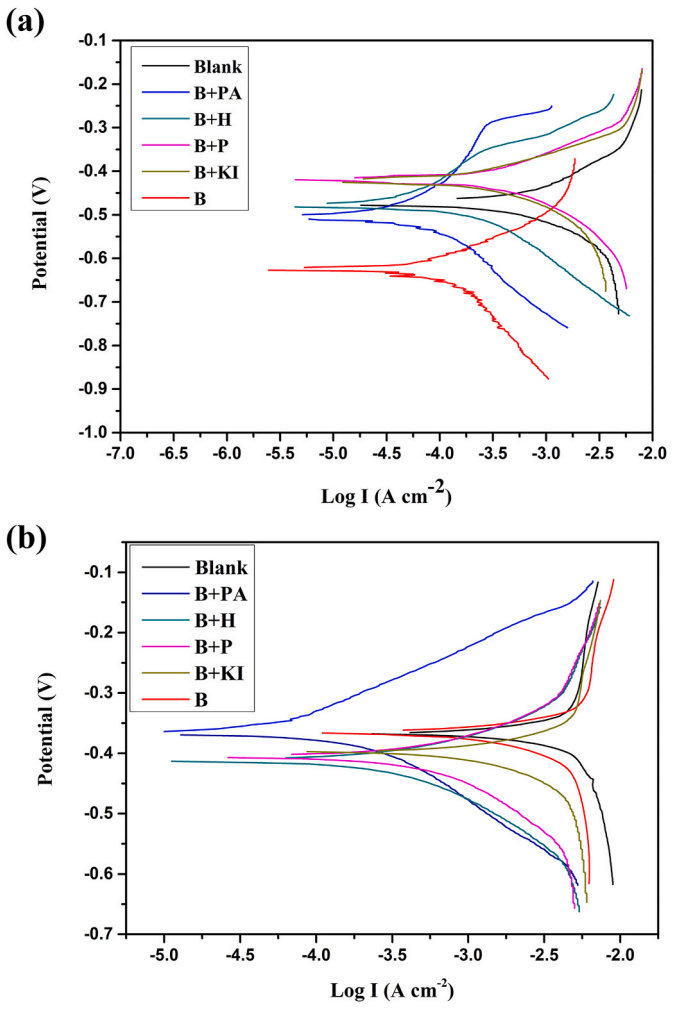

Fig. 8. PDP plots for carbon steel API P110 at 333 K in 2 M (a) and 15% (b) HCl with the blank and formulations B + PA, B + H, B + P, B + KI and B.

aggressive environment. In addition, the tests demonstrate that the potentials of all formulations are displaced from 2 M to 15% to more noble values, which is a further indication of the better performance in 15% HCl. Thus, electrochemical tests reveal the greater efficiency of formulations with acetylenic alcohols in 15% HCl.

Additionally, only one anodic reaction was observed for B + PA and B + H in 15% HCl (Fig. 8 (b)). Jayaperumal (Jayaperumal, 2010) reported two steps in the anodic reaction for carbon steel inhibition with PA in HCl at 303 and 378K, indicating that acetylenic alcohol protection is generally enhanced by the presence of iron ions (Jayaperumal, 2010). This is explained by condensation and polymerization reactions with iron ions, leading to surface films (Shemit, 1984). Given that the corrosive process is more intense in 15% HCl, the presence of iron ions is also more pronounced, which can change anodic reactions, corroborating the different mechanisms of the formulations in different acidic environments.

Peumus boldus extract (B) displaced more cathodic current densities than their anodic counterparts in the polarized region in 15% HCl, when compared to the blank. Furthermore, the combination with acetylenic alcohols improves cathodic and anodic displacements in both HCl concentrations. In relation to potentials, all formulations exhibited variations lower than 85 mV, except for B in 2 M HCl. Therefore, the active substances in the formulations can be considered mixed type inhibitors, except for B that acts as cathodic inhibitor in 2 M HCl. This demonstrates the importance of studying the performance of inhibitors in different conditions, since it may change (Prabakaran et al., 2017). In addition, the electrochemical efficiencies corroborate the gravimetric data.

3.5. Confocal laser scanning microscopy

Confocal laser scanning microscopy was performed for coupons after 15% HCl tests in the absence and presence of formulations B + PA and B + H in order to characterize the surface on localized corrosion and roughness. On each surface, at least three regions were analyzed in order to obtain the average of roughness parameters and the depth of the deepest pit (Table 10). Roughness parameter S_q indicates the root mean square height within the defined area, which would be equivalent to the standard deviation of the heights. Parameter S_a indicates the arithmetical mean height of the points within the defined area (ISO 25178-2., 2012; Qia et al., 2015). Roughness decreases significantly in the presence of the formulations, and the parameters S_q and S_a were similar for formulations B + PA and B + H, confirming their protection. In addition, Fig. 9 (a) shows an irregular surface topography and severe attack by the inorganic fluid, with a height difference of 140 μm. In the tests with B + PA and B + H (Fig. 9 (b) and (c)), a considerably more uniform surface was observed, with a topography difference of approximately 11 μm and 9 μm, respectively.

Localized corrosion was evaluated based on ASTM G48 (ASTM Standard G48-11, 2011), which recommends the precepts established by ASTM G46 (2005) (American Society for Testing and Materials, 2005). The depths of the pits were measured with 20x magnification and the deepest pit was recorded (Table 10). The penetration rate (T_p) was calculated using equation (4), where T_p is expressed in mm/y; P_{max} is the maximum depth of penetration (deepest pit), in mm; and t the test time, expressed in days.

$$T_p = \frac{P_{max} * 365}{t} \quad (4)$$

Table 10
Parameters of roughness, deepest pit depth and localized corrosion rate obtained for tests in the absence and presence of B + PA and B + H in 15% HCl at 333 K.

Test	S_q (μm)	S_a (μm)	P_{max} (mm)	T_p (mm/y)
Blank	35.210 ± 5.530	28.800 ± 4.980	–	–
B + PA	0.600 ± 0.200	0.480 ± 0.140	0.017	6.390
B + H	0.630 ± 0.050	0.480 ± 0.040	–	–

Table 9
Parameters obtained by PDP for corrosion of API P110 carbon steel in 2 M and 15% HCl without and with formulations B + PA, B + H, B + P, B + KI and B at 333 K.

	2 M					15%				
	$-E_{corr}$ (mV)	I_{corr} (μA/cm^2)	Bc (mV/dec)	βa (mV/dec)	E_{PDP} (%)	$-E_{corr}$ (mV)	I_{corr} (μA/cm^2)	Bc (mV/dec)	βa (mV/dec)	E_{PDP} (%)
Blank	471.00	14.45	14.47	19.70	–	367.00	316.22	10.00	15.00	–
B + PA	505.00	2.45	–	–	–	366.00	8.14	8.00	17.00	97.42
B + H	483.00	2.48	–	–	–	415.00	26.30	8.50	25.00	91.68
B + P	423.00	2.53	11.60	6.60	82.46	408.00	19.05	8.33	12.50	93.97
B + KI	428.00	2.34	11.60	6.60	83.78	400.00	152.76	8.93	14.28 51.69	51.29
B	632.00	3.16	10.90	3.12	78.12	366.00	186.21	9.00	16.00	41.11

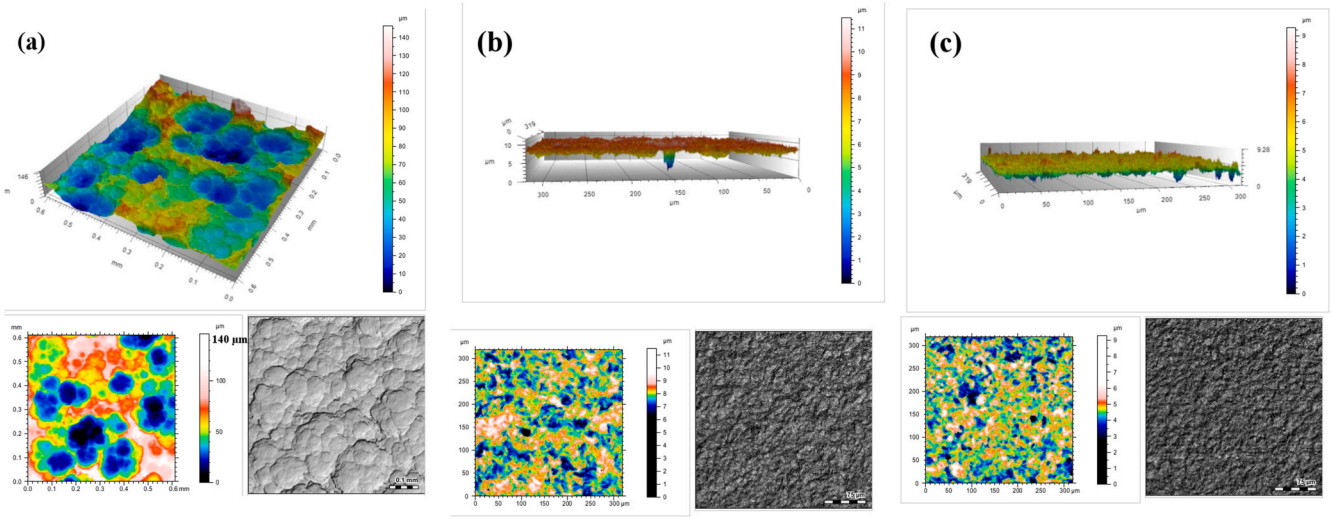

Fig. 9. Confocal laser scanning microscopy of API P110 carbon steel in the absence (a) and presence of B + PA (b) and B + H (c) after 24 h exposure at 333 K in 15% HCl.

Pits were observed only in the B + PA test, while in the B + H test, corrosion was uniform (Fig. 9). The blank test exhibited significant weight loss due to the aggressiveness of the fluid, precluding the detection of pits. According to ASTM G46 (American Society for Testing and Materials, 2005), pits with a depth of less than 25 µm represent mild localized corrosion. In addition, other literature studies approve inhibitors for application in oil well acidizing with localized corrosion below 1000 mpy (approximately 25 mm/year) (Joia et al., 2001; Nascimento, 2018). Since the rates obtained here were lower than those mentioned above, it follows that B + PA and B + H could be used in oil well acidizing up to 333 K.

3.6. SEM-EDX

SEM-EDX was performed on the specimens after removal from the acidizing cells at 333 K. The surface morphology of the coupons in the absence and presence of B + PA, B + H and B was analyzed. The presence of corrosion inhibitor on the metallic coupon, was evaluated without cleaning the analyzed surface (Fig. 10 (b), (c) and (d)).

Fig. 10 (a) shows an irregular morphology of the surface without inhibitor (blank), confirming acid attack on the metallic surface. The coupons tested with B + PA (Fig. 10 (b)) and B + H (Fig. 10 (c)) showed a less irregular morphology, confirming the protection. In addition, the darker regions correspond to the adsorbed inhibitor, confirmed by EDX.

Table 11 shows the relationship between the elements detected by EDX. The O/Fe ratio in the blank refers to oxides related to the corrosive process. The C/Fe and O/Fe ratios on the coupons after the tests with the inhibiting formulations increased significantly, due to the presence of molecules containing aromatic and oxygenated compounds. In addition, the higher O/Fe ratio present in B + PA and B + H tests is associated with the extra source of the hydroxyl group present in acetylenic compounds, confirming their adsorption along with *Peumus boldus* compounds.

3.7. FTIR-ATR

The FTIR-ATR technique can be used to confirm inhibiting functional groups on the metallic surface (Loto, 2018). The spectra of the *Peumus boldus* extract (Fig. 4(d)) obtained in the optimal condition (210 min, 343 K and 0.35 g of leaves/mL ethanol) and the inhibitory film after 24 h immersion tests with B + PA (Fig. 11(a)) and B + H (Fig. 11(b)) at 333 K were analyzed. The spectra showed bands at approximately 1600 cm^{-1} (deformation of aryl C═C substituent) and 1460 cm^{-1} (aromatic ring deformation). In addition, the B + H spectrum has a more noticeable band around 2920 cm^{-1} (symmetrical/asymmetrical stretch CH_2 methylene), and at 3350 cm^{-1}, with respect to OH deformation. Shifts in bands from *Peumus boldus* extract to those of the inhibitory film confirm the adsorption by chemical bonds on the metallic surface (Li et al., 2017). These bands are also visible in the boldo extract, confirming the adsorption of *Peumus boldus* compounds and corroborating the SEM-EDX technique.

3.8. Molecular modeling

A model based on the main alkaloid present in *Peumus boldus* extract (boldine) (Figueiredo et al., 2016; Teixeira et al., 2016) was constructed in order to analyze structural, electronic and quantum properties using calculations based on the DFT method. Fig. 12 (a) shows the optimized structure, and Fig. 12 (b) and 12 (c) show HOMO and LUMO border orbitals of the studied molecule. The HOMO and LUMO are π-type orbitals and the electron densities are displaced over the methoxyphenol groups. The planar distribution of the HOMO orbital indicates possible perfect adsorption, designating the reactive sites for the interaction. The quantum parameters, such as the energies of the highest occupied molecular orbital (E_{HOMO}) and lowest vacant molecular orbital (E_{LUMO}), the energy gap (ΔE) between E_{HOMO} and E_{LUMO}, dipole moment (µ), global electronegativity (χ), hardness (η) and softness (σ), were obtained using the corresponding optimized structure data.

Table 12 shows the quantum parameters of the boldine molecule model in its neutral form. The inhibitory effect is measured by adsorption of the molecule on the metallic surface. The energy of the highest occupied molecular orbital (E_{HOMO}) indicates the tendency of the molecule to donate electrons to low-energy receptor molecules, with an empty molecular orbital. Increasing E_{HOMO} and dipolar momentum (µ) values, and lower ΔE values favor the anticorrosive properties (Tang et al., 2009). The HOMO and LUMO energy values can be used to measure global electronegativity (χ), hardness (η) and softness (σ), according to equations (5)–(7) (Senhaji et al., 2011; Lece et al., 2008):

$$\chi = -\frac{E_{HOMO} + E_{LUMO}}{2} \quad (5)$$

$$\eta = \frac{E_{LUMO} + E_{HOMO}}{2} \quad (6)$$

$$\sigma = \frac{1}{\eta} \quad (7)$$

The boldine molecule showed an E_{HOMO} of - 5.286 eV. The quantum

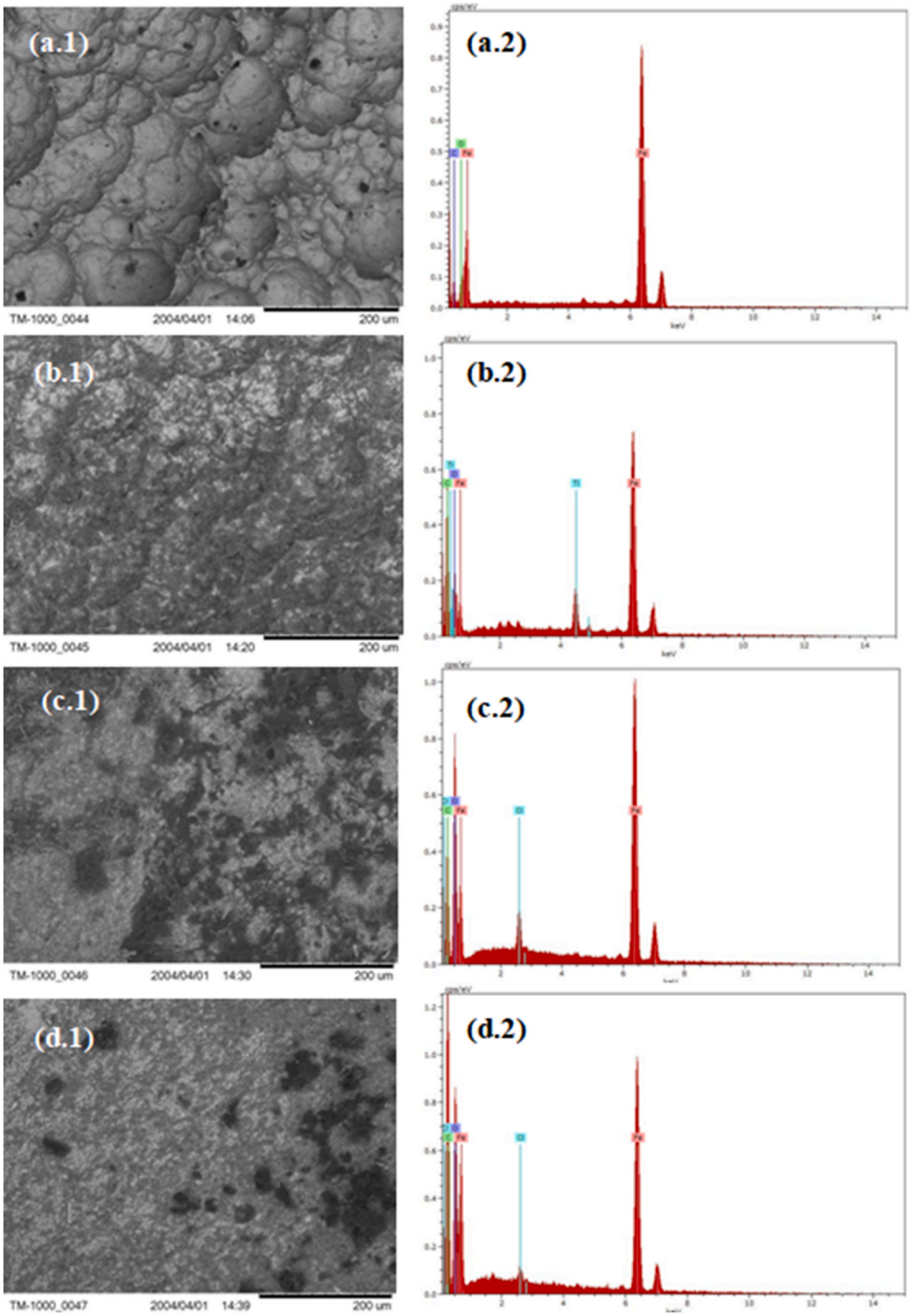

Fig. 10. SEM-EDX of API P110 carbon steel after immersion of 24 h at 333 K in 15% HCl without inhibitor ((a.1) and (a.2)) and with formulations B ((b.1) and (b.2)), B + PA ((c.1) and (c.2)) and B + H ((d.1) and (d.2)).

parameters obtained are similar to other organic molecules that demonstrated anticorrosive properties (Abdulazeez et al., 2016; Yadav et al., 2016), obtained using the same parameters as those of the theoretical calculations of this study.

Boldine was also studied in acidic media. Thus, its ability to receive protons and possible changes in its inhibitory properties were investigated by molecular modeling. The boldine structure contains heteroatoms that can be potentially protonated. The protonation energies of these compounds were calculated to determine the Lewis basic sites favorable for protonation. The variation in heteroatom protonation energy (ΔE_{prot}) was determined by the difference in protonated boldine energies ($E_{boldine}+$) and boldine molecule energy in the neutral phase ($E_{Boldine}$). The calculations follow the equation (8):

$$\Delta E_{Prot} = \Delta E_{Boldine+} - \Delta E_{Boldine} \quad (8)$$

The protonated boldine energy values are shown in Table 13. The H^+ proton remained in the boldine structure in all the heteroatoms. In all the cases studied, boldine structure remained planar and stable, favoring the adsorption. In acid solutions, the nitrogen atom will preferably be protonated, forming quaternary compounds.

The protonation of boldine improves inhibitory efficiency, compared to boldine in the gas phase, due to the decrease in the difference between

Table 11
Relation between the elements detected by SEM-EDX analysis.

Tests	Elements	%Mass	C/Fe (%)	O/Fe (%)
Blank	Fe	84.68	14.33	3.75
	C	12.14		
	O	3.18		
B	Fe	60.25	51.63	14.34
	C	31.11		
	O	8.64		
B + PA	Fe	61.56	32.37	26.99
	C	19.93		
	O	16.62		
	Cl	1.90		
B + H	Fe	44.42	80.81	42.52
	C	35.90		
	O	18.89		
	Cl	0.79		

HOMO-LUMO energies (Δ*E*). The dipole moment (μ) also increases in all the protonation possibilities of boldine. Higher dipole moment values increase the adsorption force. A decline in the E_{LUMO} energy of the protonated boldine, compared to the neutral phase inhibitor, indicates an increased capacity to receive electrons from the carbon steel. Boldine in acid solutions may act as a cathodic inhibitor (Lewis acid) in the protonated atoms, and anodic inhibitor (Lewis base) by the aromatic rings present in the molecular structure, confirming the mixed type behavior observed in electrochemical tests.

The fact that boldine acts more efficiently in electron donation to the metallic surface in acidic medium confirms the inhibitory potential. In addition, its stability was confirmed in acidic medium, indicating that it does not degrade. The increased efficiency of these formulations in a more acidic environment, as shown in the electrochemical tests, corroborates the greater electron donation of boldine when protonated. Finally, it should be noted that since the *Peumus boldus* extract contains compounds other than boldine, the reduced efficiency of formulation B in 15% HCl may correspond to activity loss of other compounds present in the mixture.

4. Conclusions

The statistical design resulted in the optimal extract, which showed an inhibition efficiency of 88.00% in 2 M HCl and 40.00% in 15% HCl at

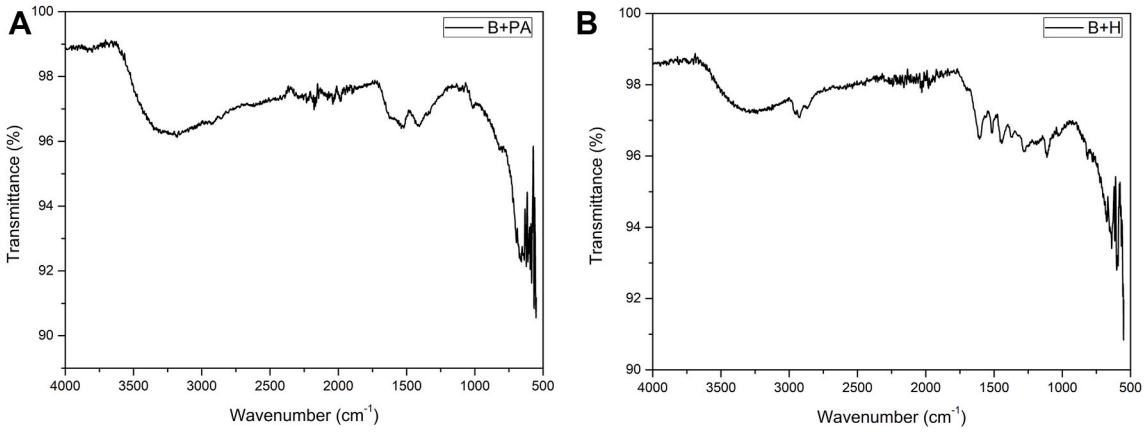

Fig. 11. FTIR-ATR of API P110 carbon steel surface after 24 h immersion at 333 K in 15% HCl with formulations B + PA (a) and B + H (b).

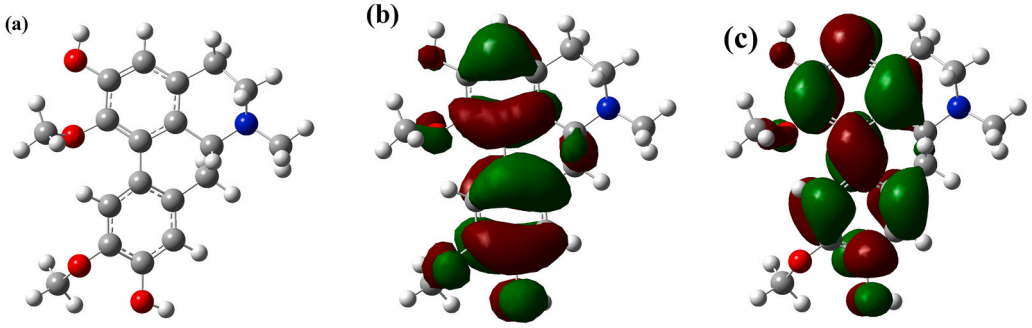

Fig. 12. (a) Optimized structure of the boldine molecule model in its neutral form, (b) the highest occupied molecular orbital and (c) the lowest vacant molecular orbital. (Red = oxygen, gray = carbon, blue = nitrogen and white = hydrogen). (For interpretation of the references to colour in this figure legend, the reader is referred to the Web version of this article.)

Table 12
Quantum parameters of the boldine and other molecules in neutral state.

Quantum properties	E_{HOMO} (eV)	E_{LUMO} (eV)	Δ*E* (eV)	*μ* (D)	*χ* (eV)	*η* (eV)	*σ* (eV^{-1})	Reference
Boldine	−5.28	−0.52	4.76	2.33	2.90	2.38	0.42	–
4MTHT*	−5.35	−1.24	4.11	2.08	–	2.05	0.24	Abdulazeez et al. (2016)
PzMBP*	−5.22	−1.37	3.84	5.25	3.30	1.92	0.52	Yadav et al. (2016)

*(4MTHT = 3,5-di (4-methylthiophenyl) -4H-1,2,4-triazole.
*PzMBP = (1 - ((piperazin-1-yl) methyl) -1H-benzo [d] imidazol-2 -yl) phenol).

Table 13
Quantum parameters of protonated boldine in different gas phase heteroatoms.

Quantum properties	E_{HOMO} (eV)	E_{LUMO} (eV)	ΔE (eV)	μ (D)	χ (eV)	η (eV)	σ (eV^{-1})	ΔE_{prot} (kcal/mol)
Boldine	−5.28	−0.52	4.76	2.33	2.90	2.38	0.42	–
N7[a]	−8.09	−3.66	4.42	13.52	5.87	2.21	0.45	−249.98
O19[a]	−8.10	−4.33	3.77	11.93	6.22	1.89	0.53	−211.05
O20[a]	−8.39	−4.32	4.06	7.78	6.36	2.03	0.49	−217.26
O21[a]	−8.07	−4.02	4.06	12.08	6.05	2.03	0.49	−217.48
O23[a]	−8.50	−4.43	4.07	4.40	6.47	2.03	0.49	−185.86

[a] Number of the protonated atom in the boldine structure (Fig. 1).

333 K. The *Peumus boldus* formulation exhibited efficiencies similar to other green inhibitors (Santos et al., 2019; Souza et al., 2016). The combination with acetylenic alcohols reduced the corrosion rate by 44.00%, confirming the possibility of partial substitution of a conventional substance by a green extract. In addition, two formulations could be used in acidizing operations up to 333 K in 15% HCl. The electrochemical tests revealed that the inhibitors are of the mixed type and that formulation with acetylenic alcohols performs better in a more acidic environment. Confocal laser scanning microscopy confirmed a more regular surface with the inhibitor and mild localized corrosion. SEM-EDX analysis confirms a less severely attacked surface with the formulations and the presence of organic inhibitory film on the metallic surface. The theoretical results showed that the methoxyphenolic groups are responsible for the adsorption on the metallic surface. Thus, the theoretical results confirm the need to maximize the phenolic content of the extracts using the statistical design. Boldine proved to be structurally stable and able to maintain protonation caused by acids. The improved inhibitory properties of boldine in acid solution were confirmed by experimental and theoretical methods. *Peumus boldus* extract produced a 13-fold decrease in the concentration of conventional inhibitors while maintaining high efficiencies.

Credit author statement

Luana B. Furtado: Conceptualization, Methodology, Validation, Investigation, Writing - Original Draft. **Rafaela C. Nascimento:** Methodology, Investigation, Validation, Writing - Review & Editing. **Maria José O. C. Guimarães:** Resources, Validation, Writing - Review & Editing. **Fábio J. F. S. Henrique:** Software, Validation, Formal analysis, Writing - Original Draft. **Janaína C. Rocha:** Validation, Formal analysis, Writing - Review & Editing, Supervision. **Peter R. Seidl:** Resources, Validation, Writing - Review & Editing. **José Antônio C. P. Gomes:** Resources, Validation, Writing - Review & Editing.

Declaration of competing interest

The authors declare that they have no known competing financial interests or personal relationships that could have appeared to influence the work reported in this paper.

Acknowledgements

The authors would like to thank E. Nunes for her assistance in the statistical design of the experiments and E. Miguez for the ^{1}H NMR analysis.

Appendix A. Supplementary data

Supplementary data to this article can be found online at https://doi.org/10.1016/j.scp.2020.100353.

Funding source

This work was supported by the Conselho Nacional de Desenvolvimento Científico e Tecnológico (CNPq) [grant number 142269/2017-4].

References

Abdulazeez, M.O., Oyebamiji, A.K., Semire, B., 2016. DFT and QSAR study of corrosion inhibition on 3,5-di-substituted pyrazole derivatives with heteroatom on position one. Leban. Sci. J. 17, 217–232.
O. Ajayi, N. Everitt, K.T. Voisey, Corrosion inhibition of mild steel in 15 wt.% HCl by durum wheat. In: European Corrosion Congress 2017 (Eurocorr 2017), 3-7 September 2017, Prague, Czech Republic.
American Society for Testing and Materials, 1972. G 31: Standard Practice for Laboratory Immersion Corrosion Testing of Metals. ASTM, West Conshohocken, p. 8, 2004.
American Society for Testing and Materials, 2005. ASTM G46-94: Standard Guide for Examination and Evaluation of Corrosion Pitting. USA.
Aribo, S., Olusegun, S.J., Ibhadiyi, L.J., Oyetunji, A., Folorunso, D.O., 2017. Green inhibitors for corrosion protection in acidizing oilfield environment. J. Assoc. Arab Univ. Basic Appl. Sci. 24, 34–38.
ASTM Standard G48-11, 2011. Standard Test Methods for Pitting and Crevice Corrosion Resistance of Stainless Steels and Related Alloys by Use of Ferric Chloride Solution. ASTM, Philadelphia.
Badea, G.E., Caraban, A., Dzitac, S., Cret, P., Setel, A., 2010. Polarisation measurements used for corrosion rates determination. J. Sustain. Energy 1, 1.
Bahlakeh, G., Ramezanzadeh, B., Dehghani, A., Ramezanzadeh, M., 2019. Novel cost-effective and high-performance green inhibitor based on aqueous Peganum harmala seed extract for mild steel corrosion in HCl solution: detailed experimental and electronic/atomic level computational explorations. J. Mol. Liq. 283, 174–195.
Barreto, L.S., Tokumoto, M.S., Guedes, I.C., Melo, H.G., Amado, F.D.R., Capelossi, V.R., 2017. Evaluation of the anticorrosion performance of peel garlic extract as corrosion inhibitor for ASTM 1020 carbon steel in acidic solution. Materia 22, e11852.
Ben Aoun, S., Bouklah, M., Khaled, K.F., Hammouti, B., 2016. Electrochemical impedance spectroscopy investigations of steel corrosion in acid media in the presence of thiophene derivatives. Int. J. Electrochem. Sci. 11, 7343–7358. https://doi.org/10.20964/2016.09.07.
Biswas, A., Pal, S., Udayabhanu, G., 2015. Experimental and theoretical studies of xanthan gum and its graft co-polymer as corrosion inhibitor for mild steel in 15% HCl. Appl. Surf. Sci. 353, 173–183.
Cherrak, K., Belghiti, M.E., Berrissoul, A., El Massaoudi, M., El Faydy, M., Taleb, M., Radi, S., Zarrou, A., Dafali, A., 2020. Pyrazole carbohydrazide as corrosion inhibitor for mild steel in HCl medium: experimental and theoretical investigations. Surf. Interfaces 20, 100578.
Coates, J., 2006. Interpretation of infrared spectra, a practical approach. Encycl. Anal. Chem. 10815–10837. https://doi.org/10.1002/9780470027318.a5606.
Dehghani, A., Bahlakeh, G., Ramezanzadeh, B., 2019a. Green Eucalyptus leaf extract: a potent source of bio-active corrosion inhibitors for mild steel. Bioelectrochemistry 130, 107339.
Dehghani, A., Bahlakeh, G., Ramezanzadeh, B., Ramezanzadeh, M., 2019b. Detailed macro-/micro-scale exploration of the excellent active corrosion inhibition of a novel environmentally friendly green inhibitor for carbon steel in acidic environments. J. Taiwan Inst. Chem. Eng. 100, 239–261.
Edelmann, A., Lendl, B., 2002. Toward the optical Tongue: flow-through sensing of Tannin−Protein interactions based on FTIR spectroscopy. J. Am. Chem. Soc. 124, 14741–14747.
El-Etre, A.Y., Ali, A.I., 2017. A novel green inhibitor for C-steel corrosion in 2.0 mol·L− 1 hydrochloric acid solution. Chin. J. Chem. Eng. 25, 373–380.
Emran, K.M., 2015. Effects of concentration and temperature on the corrosion properties of the Fe–Ni–Mn alloy in HCl solutions. Res. Chem. Intermed. 41, 3583–3596.
Falcão, A.P., Chaves, E.S., Kuskoski, E.M., Fett, R., Falcão, L.D., Bordignon-Luiz, M.T., 2007. Total polyphenol index, total anthocyanins and antioxidant activity of a model system of grape jelly. Cienc. Tecnol. Aliment. 27, 637–642.
Fernández, K., Agosin, E., 2007. Quantitative analysis of red wine tannins using Fourier-transform mid-infrared spectrometry. J. Agric. Food Chem. 55, 7294–7300.
Figueiredo, M.B.G.A., Santana, V.R., Nardelli, M.J., Nogueira, M.S., Azevedo, D.X., Santana, D.P.A., Figueiredo, A.G.A., Duarte, I.X., Junior, R.L.C.A., Lima, S.O., 2016. The effect of the aqueous extract *Peumus boldus* on the proliferation of hepatocytes and liver function in rats submitted to expanded hepatectomy. Acta Cir. Bras. 31, 608–614.
Finsgar, M., Jackson, J., 2014. Application of corrosion inhibitors for steels in acidic media for the oil and gas industry: a review. Corrosion Sci. 86, 17–41.
Frenier, W.W., Schlumberger, D., 1989. Acidizing Fluids Used to Stimulate High Temperature Wells Can Be Inhibited Using Organic Chemicals, Conference Paper. SPE International symposium on oil field chemistry, Houston, Texas, p. 111.
Frisch, M.J., Trucks, G.W., Schlegel, H.B., Scuseria, G.E., Robb, M.A., Cheeseman, J.R., Scalmani, G., Barone, V., Mennucci, B., Petersson, G.A., Nakatsuji, H., Caricato, C.,

Li, X., Hratchiean, H.P., Izmaylov, A.F., Bloino, J., Zheng, G., Sonnenberg, J.L., Hada, M., Ehara, M., Toyota, K., Fukuda, R., Hasegawa, J., Ishida, M., Nakajima, T., Honda, Y., Kitao, O., Nakai, H., Vreven, T., Montgomery, J.A., Peralta, J.E., Ogliaro, F., Bearpark, M., Heyd, J.J., Brothers, E., Kudin, K.N., Staroverov, V.N., Kobayashi, R., Normand, J., Raghavachari, K., Rendell, A., Burant, J.C., Iyengar, S. S., Tomasi, J., Cossi, M., Rega, N., Millam, J.M., Klene, M., Knox, J.E., Cross, J.B., Bakken, V., Adamo, C., Jaramillo, J., Gomperts, R., Stratmann, R.E., Yazyev, O., Austin, A.J., Cammi, R., Pomelli, C., Ochterski, J.W., Martin, R.L., Morokuma, K., Zakrzewaki, V.G., Voth, V.A., Salvador, P., Dannenberg, J.J., Dapprich, S., Daniels, A.D., Farkas, O., Foresman, J.B., Ortiz, J.V., 2009. GAUSSIAN 09, Revision A.2. Gaussian Inc., Wallingford, CT, USA.

Funkhouser, G.P., Cassidy, J.M., Lane, J.L., Frost, K., Gardner, T.R., king, K.L., 2001. US Patent 6192987B1 published on February.

Furtado, L.B., Rocha, J.C., Gomes, J.A.C.P., Nascimento, R.C., Seidl, P.R., José, M., Guimarães, O.C., Tonon, R.V., Cabral, L.M.C., Mattos, G.N., 2020. Storage time evaluation of a residue from wine industry as a microencapsulated corrosion inhibitor for 1 M HCl. Mater. Chem. Phys. 256, 123739.

Golestani, Gh, Shahidi, M., Ghazanfari, D., 2014. Electrochemical evaluation of antibacterial drugs as environment-friendly inhibitors for corrosion of carbon steel in HCl solution. Appl. Surf. Sci. 308, 347–362.

Gowraraju, N.D., Jagadeesan, S., Ayyasamy, K., Olasunkanmi, L., Ebenso, E.E., Subramanian, C., 2017. Adsorption characteristics of Iota-carrageenan and Inulin biopolymers as potential corrosion inhibitors at mild steel/sulphuric acid interface. J. Mol. Liq. 232, 9–19.

Hill, D.G., 2014. Patent WO 2014/149306 Al published on September.

Holze, L.R.B., 2005. Electrochemical Behavior of Aluminum in Ethylene Glycol-Water Mixtures. Effect of Addition of Chelating Agents. Thesis (Doctorate in Chemistry). Federal University of Rio Grande do Sul.

ISO 25178-2., 2012. Geometrical Product Specifications (GPS) - Surface Texture: Areal - Part 2: Terms, Definitions and Surface Texture Parameters. International Organization for Standardization.

Ituen, E., James, A., Akaranta, O., Sun, S., 2016. Eco-friendly corrosion inhibitor from Pennisetum purpureum biomass and synergistic intensifiers for mild steel. Chin. J. Chem. Eng. 24, 1442–1447.

Jayaperumal, D., 2010. Effects of alcohol-based inhibitors on corrosion of mild steel in hydrochloric acid. Mater. Chem. Phys. 119, 478–484.

Joia, C.J.B.N., Brito, R.F., Barbosa, B.C., Moraes, F.D., Pereira, A.Z.I., Marques, L.C.C., 2001. Corrosion. NACE International, Houston, Texas paper 01007.

Juttner, K., 1990. Electrochemical impedance spectroscopy (EIS) of corrosion processes on inhomogeneous surfaces. Electrochim. Acta 35, 1501–1508.

Keramatinia, M., Ramezanzadeh, B., Mahdavian, M., 2019. Green production of bioactive components from herbal origins through one-pot oxidation/polymerization reactions and application as a corrosion inhibitor for mild steel in HCl solution. J. Taiwan Inst. Chem. Eng. 105, 134–149.

Lece, H.D., Emregul, K.C., Atakol, O., 2008. Difference in the inhibitive effect of some Schiff base compounds containing oxygen, nitrogen and sulfur donors. Corrosion Sci. 50, 1460–1468.

Li, F., Shengtao, Z., Song, Y., Shenying, X., Shijin, C., 2017. Experimental and theoretical studies of 1-vinyl-3- hexylimidazolium iodide ([VHIM]I) as corrosion inhibitor for the mild steel in sulfuric acid solution. Int. J. Electrochem. Sci. 12, 1915–1928. https://doi.org/10.20964/2017.03.30.

Loto, R.T., 2018. Electrochemical analysis of the corrosion inhibition properties of L-leucine and trypsin complex admixture on high carbon steel in 1 M H_2SO_4 solution. Rev. Colomb. Quím. 47, 12–20. https://doi.org/10.15446/rev.colomb.quim.v47n2.68058.

Mariano, X.M., 2015. Evaluation of the Chemical Composition of the Essential Oil of Commercial Samples of Boldo-Do-chile (*Peumus boldus* Molina). Dissertation (Master in Food and Nutrition). Federal University of the State of Rio de Janeiro.

McCafferty, E., 2005. Validation of corrosion rates measured by the Tafel extrapolation method. Corrosion Sci. 47, 3202–3215.

Menezes, M.A.M., Valle, M.L.M., Dweck, J., Queiroz, J.C., 2007. Temperature dependence of corrosion inhibition of steels used in oil well stimulation using acetylenic compound and halide ion salt mixtures. Braz. J. Petrol. Gas 1, 8–15.

Mesher, S., 2006. US Patent 20060046939A1 published on March.

Mishra, A., Verma, C., Lgaz, H., Srivastava, V., Quraishi, M.A., Ebenso, E.E., 2018. Synthesis, characterization and corrosion inhibition studies of N-phenyl-benzamides on the acidic corrosion of mild steel: experimental and computational studies. J. Mol. Liq. 251, 317–332.

Mobin, M., Zehra, S., Parveen, M., 2016. L-Cysteine as corrosion inhibitor for mild steel in 1 M HCl and synergistic effect of anionic, cationic and non-ionic surfactants. J. Mol. Liq. 216, 598–607.

Nascimento, R.C., 2018. Development of organic formulations for oil well acidification fluids. In: Doctoral Thesis in Chemical and Biochemical Process Technology. School of Chemistry, Federal University of Rio de Janeiro.

Obot, I.B., Obi-Egbedi, N.O., 2010. Theoretical study of benzimidazole and its derivatives and their potential activity as corrosion inhibitors. Corrosion Sci. 52, 657–660.

Oliveira, G.S., 2002. Evaluation of Potential Corrosion Inhibitors of Steel for Acidizing Operations in Oil Well. Dissertation. Federal university of Rio de Janeiro.

Oliveira, M.C.C., Carvalho, M.G., Ferreira, D.T., Braz-Filho, R., 1999. Flavonoides das flores de *Stiffitia chrysantha* Mikan. Quim. Nova 22, 182–184.

Pavia, D.L., Lampman, G.M., Kriz, G.S., 1996. Infrared Spectroscopy. Saunder college publishing, Estados Unidos, pp. 14–95.

Pereira, S.S.A.A., Pêgas, M.M., Fernández, T., Magalhães, T.M., Schöntag, T.G., Lago, D. C., Senna, L.F., D'Elia, E., 2012. Inhibitory action of aqueous garlic peel extract on the corrosion of carbon steel in HCl solution. Corrosion Sci. 65, 360–366.

Pires, L.F., Brinatti, A.M., Saab, S.C., 2015. Experimental method to determine some physical properties in physics classes, R. Bras. Ci. SOLO 39, 1507–1512.

Pourbaix, M., 1973. Lectures on electrochemical corrosion, translated from the French by. In: Green, J.A.S., Staehle, R.W. (Eds.), Foreword by Jerome Kruger. Pleunum Press, New York, pp. 213–214. CEBELCOR, Brussels.

Prabakaran, M., Kim, S., Mugila, N., Hemapriya, V., Parameswari, K., Chitra, S., Chung, I., 2017. Aster koraiensis as nontoxic corrosion inhibitor for mild steel in sulfuric acid. J. Ind. Eng. Chem. 52, 235–242.

Qia, Q., Li, T., Scott, P.J., Jiang, X., 2015. A correlational study of areal surface texture parameters on some typical machined surfaces. Procedia CIRP 27, 149–154.

Raghavendra, N., Bhat, J.I., 2018. Red arecanut seed extract as a sustainable corrosion inhibitor for aluminum submerged in acidic corrodent: an experimental approach towards zero environmental impact. Period. Polytech. - Chem. Eng. 62, 351–358.

Rajeev, P., Surendranathan, A.O., Murthy, C.S.N., 2012. Corrosion mitigation of the oil well steels using organic inhibitors – a review. J. Mater. Environ. Sci. 3, 856–869.

Ruiz, A.L.T.G., Taffarello, D., Souza, V.H.S., Carvalho, J.E., 2008. Farmacologia e toxicologia de *Peumus boldus* e Baccharis genistelloides. Rev. Bras. Farmacogn. 18, 295–300.

Santos, E.C., Cordeiro, R., Santos, M., Rodrigues, P.R.P., Singh, A., D'Elia, E., 2019. Barley agro-industrial residues as corrosion inhibitor for mild steel in 1mol L^{-1} HCl solution. Mater. Res. 22, e20180511 https://doi.org/10.1590/1980-5373-MR-2018-0511.

Seidl, P.R., Menezes, S.M.C., Baptista, I.P., Guimarães, M.J.O.C., Pereira, E.A., Moura, M. B.R., 2011. Corrosion Inhibiting Composition of Petroleum Well Acidizing Process Patent Number Nº PI 1101070-3 A2 published on June 04.

Senhaji, O., Taouil, R., Skalli, M.K., Bouachrine, M., Hamidi, M., Hammouti, B., Al-Deyab, S.S., 2011. Experimental and theoretical study for corrosion inhibition in normal hydrochloric acid solution by some new phophonated compounds. Int. J. Electrochem. Sci. 6, 6290–6299.

Shemit, G., 1984. Application of inhibitors for acid media: report prepared for the European federation of corrosion working party on inhibitors. Br. Corrosion J. 19, 165–176.

Singh, M.R., Gupta, P., Gupta, K., 2019. The litchi (Litchi Chinensis) peels extract as a potential green inhibitor in prevention of corrosion of mild steel in 0.5 M H2SO4 solution. Arab. J. Chem. 12, 1035–1041.

Souza, E.C.C.A., Ripper, B.A., Perrone, D., D'Elia, E., 2016. Roasted coffee extracts as corrosion inhibitors for mild steel in HCL solution. Mater. Res. 19, 1276–1285.

Tang, Y.M., Yang, W.Z., Yin, X.S., Liu, Y., Wan, R., Wang, J.T., 2009. Phenyl-substituted amino thiadiazoles as corrosion inhibitors for copper in 0.5 M H_2SO_4. Mater. Chem. Phys. 116, 479–483.

Teixeira, C.C.C., Cabral, T.P.F., Sousa, J.P.B., Teixeira, S.P., Bastos, J.K., Freitas, L.A.P., 2016. Study of quality assurance for *Peumus boldus* m products by botanic profiling, extraction optimization, HPLC quantification and antioxidant assay. Phcog. J. 8, 264–272.

Umoren, S.A., Eduok, U.M., 2016. Application of carbohydrate polymers as corrosion inhibitors for metal substrates in different media: a review, Carbohyd. Polym 140, 314–341.

S. A. Umoren, M. M. Solomon, I. B. Obot, R. K. Suleiman, Comparative studies on the corrosion inhibition efficacy of ethanolic extracts of date palm leaves and seeds on carbon steel corrosion in 15% HCl solution, J. Adhes. Sci. Technol., DOI: 10.1080/01694243.2018.1455797.

Wang, Q., Tan, B., Bao, H., Xie, Y., Mou, Y., Li, P., Chen, D., Shi, Y., Li, X., Yang, W., 2019. Evaluation of Ficus tikoua leaves extract as an eco-friendly corrosion inhibitor for carbon steel in HCl media. Bioelectrochemistry 128, 49–55.

Williams, D.A., McDougall, L.A., Looney, J.R., 1996. US Patent 5543388A published on August.

Yadav, M., Kumar, S., Purkait, T., Olasunkanmi, L.O., Bahadur, I., Ebenso, E.E., 2016. Electrochemical, thermodynamic and quantum chemical studies of synthesized benzimidazole derivatives as corrosion inhibitors for N80 steel in hydrochloric acid. J. Mol. Liq. 213, 122–138.

Ye, Y., Yang, D., Chen, H., 2019. A green and effective corrosion inhibitor of functionalized carbon dots. J. Mater. Sci. Technol. 35, 2243–2253.

Ye, Y., Zou, Y., Jiang, Z., Yang, Q., Chen, L., Guo, S., Chen, H., 2020a. An effective corrosion inhibitor of N doped carbon dots for Q235 steel in 1 M HCl solution. J. Alloys Compd. 815, 152338.

Ye, Y., Yang, D., Chen, H., Guo, S., Yang, Q., Chen, L., Zhao, H., Wang, L., 2020b. A high-efficiency corrosion inhibitor of N-doped citric acid-based carbon dots for mild steel in hydrochloric acid environment. J. Hazard Mater. 381, 121019.

Ye, Y., Zhang, D., Zou, Y., Zhao, H., Chen, H., 2020c. A feasible method to improve the protection ability of metal by functionalized carbon dots as environment-friendly corrosion inhibitor. J. Clean. Prod. 264, 121682.